



# Effect of Hydrostatic Pressure on the Revers Gate-Current of AlGa<sub>N</sub>/Ga<sub>N</sub> HEMTs

Rajab Yahyazadeh<sup>1\*</sup>, Zahra Hashempour<sup>1</sup>

<sup>1</sup>Department of Physics, Khoy Branch,  
Islamic Azad University, Khoy, IRAN

\*Corresponding Author

DOI: <https://doi.org/10.30880/ijie.2021.13.05.028>

Received 09 July 2020; Accepted 07 June 2021; Available online 24 November 2021

**Abstract:** In this paper, we present an Analytical-Numerical model for reverse gate leakage current in AlGa<sub>N</sub>/Ga<sub>N</sub> high electron mobility transistors (HEMTs), which investigate the influence of the hydrostatic pressure (HP) on gate-current. Salient features of the model are incorporated of occupied sub-bands in the interface quantum well, combined with a self-consistent solution of the Schrödinger and Poisson equations. Finite difference techniques have been used to acquire energy eigenvalues and their corresponding eigenfunctions of AlGa<sub>N</sub>/Ga<sub>N</sub> (HEMTs). It has been found that the bound charge at the heterointerface has the most impact on the threshold voltage. The increases in hydrostatic pressure cause an increase in threshold voltage. With increasing HP, the Schottky barrier height decreases, AlGa<sub>N</sub> electric field and reverse gate leakage current are increased. The increase in HP acts as a positive virtual gate. The dependence on the HP of Poole-Frenkel emission (FP) and Fowler-Nordheim (FN) direct tunneling is more than trap-assisted-tunneling (TAT). Increasing the pressure of 2GPa, the intersection point of PF and TAT varies by 1 volt, the reverse gate current increases by an average of 35%, and the threshold voltage increases to 1.15 V in absolute terms.

**Keywords:** Gate current, hydrostatic pressure, AlGa<sub>N</sub>/Ga<sub>N</sub> HEMT

## 1. Introduction

AlGa<sub>N</sub>/Ga<sub>N</sub> high electron mobility transistor (HEMT) devices are considered to be very promising candidates for high-speed and high-power applications [1, 2]. These devices offer advantages such as high breakdown voltage, high charge density, and good electron mobility [3-5]. Tunneling of electrons across barriers offers very fast-state switching capability, which enhances the high-frequency switching performance of electronic devices. There are several tunneling phenomena, such as Fowler-Nordheim (FN) direct tunneling, trap-assisted tunneling (TAT), thermionic field-emission (TFE), and trap-assisted Frenkel-Poole (FP) emission, in nitride heterojunctions [6, 7]. The pressure was not analyzed in the calculation of gate leakage current components and its physical parameters by Mojaver et al. [8] and Turuvekere et al. [9]. The density of the well-electron, surface density, and electric field are required to calculate the dependence of the hydrostatic pressure gate leakage current. The formation of the 2-D electron gas (2DEG) in these devices is the heart of the device operation and has been studied in great detail in the literature. Considering the high degree of application of transistors in electronic components, the effect of hydrostatic pressure is important on its performance. The external mechanical stress test on these transistors was carried out by [10]. In this paper, the effect of hydrostatic pressure is accurately investigated on the electric field in AlGa<sub>N</sub> barrier ( $E_b$ ), bound charge at the heterointerface ( $\sigma_b$ ), Schottky barrier-height ( $\phi_B$ ), threshold voltage ( $V_T$ ), electron density in quantum well, and gate leakage current components. Therefore, the dependence on the hydrostatic pressure of the parameters, such as the threshold voltage, the bond charge at hetrointerface ( $\sigma_b$ ), the band gaps, the dielectric constants, the Schottky barrier height, and the thickness of the barrier, are separately evaluated here. In the one-dimensional numerical simulations, the

experimental results, material and device details, and all other material parameters have been taken from Refs. 9 and 11-13 for HEMTs. The most important advantage of this Analytical- numerical method and the aspect of innovation in this work is the use of five important parameters, including effective mass, energy gap, lattice constants, dielectric constant and quantum barrier, and well thickness, all of which are simultaneously dependent on hydrostatic pressure and temperature. In this model, the conduction band energy, wave functions, and energy subbands are obtained from the self-consistent solution of the Schrodinger and Poisson equations. It should be noted that in this work atmospheric pressure is associated with hydrostatic pressure ( $P = P_{hydro} + P_{atm}$ ). That is, at zero hydrostatic pressure is the only atmospheric pressure applied and the fringing-field effect can be ignored. In fact, to solve the Schrödinger-Poisson equation at low temperatures, the electric fields resulting from the piezoelectric ( $P_{PZ}$ ) and spontaneous polarization ( $P_{SP}$ ) charges (which are temperature-independent) are greater than the thermionic field-emission (temperature-dependent). In this model, therefore, thermionic field-emission plays a smaller role at a low temperature range, hence it is neglected here.

## 2. Device Structure

One-dimensional numerical simulations of the  $Al_xGa_{1-x}N/GaN$  HEMT were performed using the structure illustrated in Figure 1, where the x-direction is along the 2DEG channel, the z-direction is along the growth direction, and the regions I and III represent the ungated channel portions of the HEMT. The structure consists of an undoped GaN layer to form the 2DEG channel, an undoped AlGaN spacer layer ( $d_s$ ), an n-doped AlGaN layer of the thickness ( $d_a$ ), and an undoped Schottky cap layer of the thickness. In general, the thickness of the AlGaN layer is equal to  $d_{AlGaN} = d_s + d_i + d_a$ . To compare with experimental data, it should be notified that the structure parameters may vary with the existing experimental data, that is, the ( $d_s$ ) and ( $d_i$ ) may be neglected. The conduction band diagram on the left side shows the position of the quantum well ( $z=0$ ) formation. The gate is a Ni/Pt alloy deposited on a thin AlGaN layer of the typical thickness (24 nm) and an AlN spacer layer of  $1 \mu m$  while the thickness of the underlying GaN layer is about  $2 \mu m$  [9]. This causes the AlGaN layer to be completely depleted of mobile charge carriers due to the overlap of the depletion regions at the metal/AlGaN interface (Schottky contact) and the AlGaN/GaN heterostructure interface. The gate length, source-to-gate spacing, and source-to-drain spacing are 4, 10, and  $30 \mu m$ , respectively. Source and drain lengths ( $L_S, L_D$ ) are taken to be  $2 \mu m$  each, and Al mole fraction (m) is 26%.

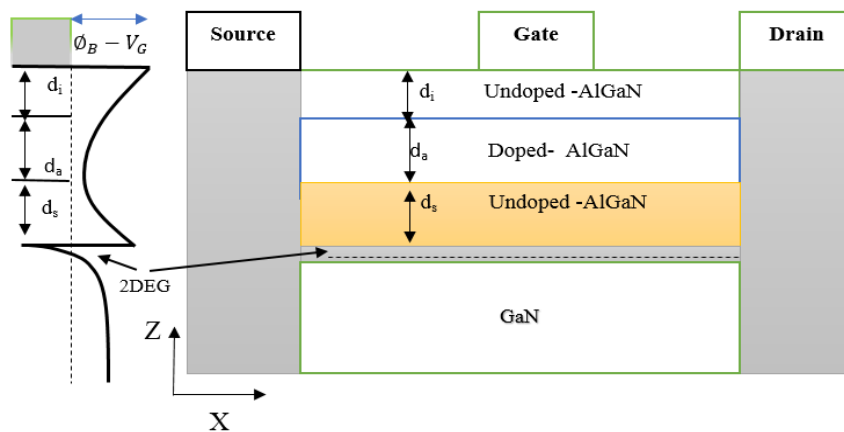


Fig. 1 - Schematic diagram of  $Al_xGa_{1-x}N/GaN$  HEMT

## 3. Modeling HEMT

### 3.1 Self-consistent Solution of Schrödinger-Poisson Equations

In order to obtain accurate values for the Fermi energy, the energies of quantized levels within the 2DEG, potential profiles, wave function and the sheet carrier concentration for the 2DEG in AlGaN/GaN heterostructures; both the Schrödinger and Poisson equations must be solved self-consistently. This has been achieved by solving Schrödinger's equation and simultaneously taking into account the electrostatic potential obtained from Poisson's equation, as well as the image and exchange-correlation potentials using three-point finite difference method. The Schrodinger equation is introduced to solve the wave function of electrons in the quantum structures:

$$-\frac{\hbar^2}{2m_e^*} \nabla^2 \psi_n + V \psi_n = E_n \psi_n \quad (1)$$

where  $\hbar$  represents the reduced Planck constant,  $m_e^*$  electron effective mass,  $V$  the potential function,  $\psi_n$  the nth state wave function, with its associated nth state energy level  $E_n$ . The electron effective mass  $m_e^*$  can be written as [11]

$$\frac{m_0}{m_e^*(P, T, m)} = 1 + \frac{E_p^\Gamma (E_g^\Gamma(P, T, m) + 2\Delta_{S0} / 3)}{E_g^\Gamma (E_g^\Gamma(P, T, m) + \Delta_{S0})} \quad (2)$$

where  $m_0$  is the free electron mass,  $E_p^\Gamma$  is the energy linked to the momentum matrix element,  $\Delta_{S0}$  is the spin-orbit splitting and  $E_g^\Gamma(P, T, m)$  is the band gap variation as a function of the hydrostatic pressure and temperature.  $E_g^{AlGaN}$ , is given by [12-14]

$$E_g^{AlGaN}(T, P) = xE_g^{AlN}(T, P) + (1-x)E_g^{GaN}(T, P) - x(1-x) \quad (3)$$

where  $E_g^{AlGaN}$  is the band gap from  $E_g^{AlN}(T, P)$  and  $E_g^{GaN}(T, P)$  respectively, as follows [13]

$$E_g(T, P) = E_g(0, 0) + \gamma P + \sigma P^2 + \frac{\alpha T^2}{T + T_e} \quad (4)$$

$E_g(0, 0)$ , stands for the band gap energy of GaN or AlGaN in the absence of the hydrostatic pressure and at a temperature 0 K. The suggested parameters used in Eq. (4) in our calculations have been taken from Ref 11. The Poisson equation relates the electrostatic potential with spatial charge distribution and it is written as

$$\kappa \nabla^2 \phi = -\rho + \nabla P_{tot} \quad (5)$$

where  $\phi$  is the potential distribution and  $\rho$  is the net charge which is a nonlinear function of the potential:

$$\rho(\phi) = [p(\phi) + n(\phi) + N_D^+ - N_A^-] \quad (6)$$

$p$  and  $n$  denote the mobile carrier density of holes and electrons,  $N_D^+$  and  $N_A^-$  are the totally ionized donor and acceptor densities.  $P_{tot} = P_{SP} + P_{PZ}$ , denotes the total polarization vector that is composed of spontaneous polarization and strain-induced piezoelectric polarization. Using the correction between composition  $m$ , band gap, lattice constant  $a$  and the strain ( $\delta$ ), they are given as follow [15, 16]

$$P_{GaN}^{PZ} = -0.918\delta + 9.541\delta^2 \quad (7)$$

$$P_{AlN}^{Pz} = \begin{cases} -1.808\delta + 5.624\delta^2 & \text{for } \delta < 0 \\ -1.808\delta - 7.888\delta^2 & \text{for } \delta > 0 \end{cases}$$

$$P_{AlGaN}^{SP} = 0.090m - 0.034(1-m) + 0.21x(1-m)$$

The strain is expressed from the lattice of substrate  $a_s$  and the epilayer  $a_e(T, P, m)$ :

$$\delta(T, P, m) = \frac{a_c - a_e(T, P, m)}{a_e(T, P, m)} \quad (8)$$

The lattice constants as function of temperature, alloy and the hydrostatic pressure is given by [17, 18]

$$a_e(T, P, m) = a_0(m) \left[ \left( 1 + \beta(T - T_{ref}) \right) \left( 1 - \frac{P}{3B_0} \right) \right] \quad (9)$$

where  $B_0 = 239 \text{ GPa}$  is the bulk modulus of sapphire.  $\beta_{GaN} = 5.56 \times 10^{-6} \text{ K}^{-1}$  is the thermal expansion coefficient and  $T_{ref} = 300 \text{ K}$ .  $a_0(m)$ , is the equilibrium lattice constant as a function of composition is given by [19, 20]

$$a_0(m) = 0.13989m + 0.03862 \quad (10)$$

The piezoelectric polarization is defined by Vegard's law as

$$P_{AlGaN}^{Pz} = mP_{AlN}^{Pz} + (1-m)P_{GaN}^{Pz} \quad (11)$$

The total polarization at the interface AlGaN/GaN is expressed as:

$$\sigma_b(T, P, m) = \left| P_{Al_mGa_{1-m}N}^{Pz} + P_{Al_mGa_{1-m}N}^{SP} - P_{GaN}^{SP} - P_{GaN}^{Pz} \right| \quad (12)$$

### 3.2 Electron Concentration

Using Self-consistent solution of Schrödinger-Poisson equations, the energy of each subband  $E_i$  is obtained. Knowing the  $E_i$ , the two ( $n_{2D}$ ), three-dimensional ( $n_{3D}$ ) and total density of electrons ( $n_S = n_{2D} + n_{3D}$ ) can be calculated from these set of equations [21, 22, 23]

$$n_{2D} = \sum_i \frac{m^* k_B T}{\pi \hbar^2} \ln \left[ 1 + \exp \left\{ \frac{(E_f - E_i)}{k_B T} \right\} \right] |\psi_i|^2 \quad (13)$$

$$n_{3D} = \frac{2}{\sqrt{\pi} N_C F_{1/2} \left( (E_F - E_C) / k_B T \right)} \quad (14)$$

$$n_{2D}(T, m, x, P) = \frac{\epsilon_0 \epsilon(m, T, P)}{(d_d(T, P) + d_i + \Delta d)} (V_{GS} - V_T - E_F - V_{CH}(x)) \quad (15)$$

Here,  $F_{1/2}$  is Fermi integral of order 1/2,  $V_T$  is the threshold voltage,  $\epsilon^{GaN}(T, P)$  and  $\epsilon^{AlGaN}(m, T, P)$  are the dielectric constant [24, 25],  $d_{AlGaN}$  is the AlGaN barrier thickness and they are given by [12-25]:

$$V_T = \phi_B - \Delta E_C(m, T, P) - \frac{\sigma_{Pz}(m, T, P) d_{AlGaN}(P, T)}{\epsilon_0 \epsilon_{AlGaN}(m, T, P)} - \frac{q N_D d_{AlGaN}^2(P, T)}{\epsilon_0 \epsilon_{AlGaN}(m, T, P)} \quad (16)$$

where  $\phi_B$  is the Schottky barrier-height and  $\Delta E_C$  is the conduction band offset between AlGaN and GaN. Here,  $\epsilon_{GaN}(T, P)$ , and  $\epsilon_{InGaN}(m, T, P)$  are the dielectric constant of the GaN and AlGaN, and  $d_{Al_mGa_{1-m}N}(T, P)$  is the thickness of AlGaN so that they are given by [12, 24, and 25]:

$$\epsilon_{GaN}(T, P) = 10.28 \times \exp \left( 10^{-4} (T - T_0) - 6.7 \times 10^{-3} P \right) \quad (17)$$

$$\epsilon_{AlGaN}(m, T, P) = \epsilon^{GaN}(T, P) + 0.03m \quad (18)$$

$$d_{Al_mGa_{1-m}N}(T, P) = d_{AlGaN}(0) \left[ 1 - \left( S_{11}^{Al_mGa_{1-m}N} + 2S_{12}^{Al_mGa_{1-m}N} \right) P \right] \quad (19)$$

Here,  $d_{AlGaN}(0)$  is the AlGaN layer thickness without hydrostatic pressure and temperature.  $S_{11}$ ,  $S_{12}$  are the elastic compliance constants of  $Al_mGa_{1-m}N$  and they are given by [11, 25]:

$$S_{11} = \frac{C_{11}C_{33} - C_{13}^2}{(C_{11} - C_{12}) [C_{33}(C_{11} + C_{12}) - 2C_{13}^2]} \quad (20)$$

$$S_{12} = \frac{C_{12}C_{33} - C_{13}^2}{(C_{11} - C_{12}) [C_{33}(C_{11} + C_{12}) - 2C_{13}^2]}$$

$V_{CH}(x)$ , is the channel potential and  $\Delta d_{2DEG} = 1/n_{2D} \int z n_{2D}(z) dz$  represents the effective width of the 2DEG channel [20]. It should be mentioned that to calculate the conduction band offset in AlGaN/GaN interface, the temperature and hydrostatic pressure dependence of energy band gap has been taken into account as [13]:

$$\Delta E_C(T, P) = 0.75 \left( E_g^{AlGaN}(T, P) - E_g^{GaN}(T, P) \right) \quad (21)$$

### 3.3 Electric field in the AGaN Layer

The electric field in the AGaN layer near the heterointerface is given by [26, 27]:

$$E_b(P, T, m) = \frac{\sigma_b(T, P, m) - n_s}{\epsilon_{eff}} \quad (22)$$

$$\epsilon_{eff} = \frac{e_{33}^2}{C_{33}} + \epsilon_{AlGaN}$$

In the calculations presented in this section determining  $E_b$  and Schottky barrier-height ( $\phi_B$ ) follow an iterative approach, as  $E_b$  and  $\phi_B$  are mutually dependent. The dependencies Schottky barrier-height to  $E_b$  and T are as follows [28]:

$$\phi_B = \phi_{B0} - 0.4 \times \sqrt{\frac{qE_b}{4\pi\epsilon_{AlGaN}}} - 2.7 \times 10^{-4} T \quad (23)$$

$$\phi_{B0} = 1.3m + 0.84$$

In the first iteration  $\phi_b$  is calculated assuming zero electric-field, followed by the recalculation of  $E_b$ . This procedure continues until convergence. It should be mentioned that the discussed leakage components are those which are responsible for leakage from gate to the 2DEG, hence excluding surface leakage. This is in agreement with the choice of  $V_{DS} = 0V$  and moderate values for  $V_{GS}$ .

### 4. Gate-Current

We regard gate leakage current ( $I_G$ ) to arise from four current components, i.e., Fowler-Nordheim (FN) direct tunneling, trap-assisted tunneling (TAT), thermionic field-emission (TFE), and trap-assisted Frenkel-Poole (FP) emission. Thus, we have the total gate current as [9]:

$$I_G = S \times (J_{FN} + J_{TAT} + J_{FP} + J_{TFT}) \quad (24)$$

where S is the gate area. In the presence of an electric-field across the barrier, electrons can tunnel through the AlGaN layer (from the metal Fermi level to the conduction-band of GaN) via the FN tunneling process. According to this process, the current density is given by [28, 29]:

$$J_{FN}(P, T, m) = \frac{q^2 (m_0 / m_{AlGaN}^*(T, P))}{8\pi h \phi_b} E_b^2(P, T, m) \exp\left(-\frac{8\pi\sqrt{2m_{AlGaN}^*(P, T)}}{3hE_b(P, T)} \phi_b^{3/2}\right) \quad (25)$$

in which  $q$  is the fundamental electronic charge and  $h$  is the Planck constant.

Tunneling may also occur via TFE when thermally energized electrons rise to higher energy levels, from where they tunnel through the thinner physical barrier. According to TFE, the current density is given by [28]:

$$J_{TFE}(P, T, m) = \frac{qA^*}{k} \int_0^{\phi_b} \frac{1}{1 + \exp[q(\phi_b - \phi) / kT]} \exp\left(-\frac{8\pi\sqrt{2m_{AlGaN}^*(P, T)}}{3hE_b(P, T, m)} \phi_b^{3/2}\right) d\phi \quad (26)$$

in which  $A^*$  is the Richardson constant and  $k$  is the Boltzmann constant.

In the case of carrier transport via traps, two main mechanisms are usually considered, one of which is the PF electron emission from metal (or a trap level in the barrier very close to the metal Fermi level) into a continuum of states in the barrier associated with a conductive dislocation. It is through this continuum of states that electrons can directly transport to the GaN channel. The PF current density is accordingly explained by [27]:

$$J_{PF}(P, T, m) = C_{PF} E_b(P, T, m) \exp\left(-\frac{q(\phi_{t-PF} - \sqrt{qE_b(P, T, m) / \pi\epsilon_0\epsilon_{AlGaN}(P, T, m)})}{kT}\right) \quad (27)$$

in which  $q\phi_{t-PF}$  is the barrier height for electron emission from the trap state, and  $C_{PF}$  is a constant.

Actually, PF emission means the electron emission from the trap by thermal activation but with a lowered trap depth induced by the Coulomb interaction, i.e., the emission rate enhanced by the electric field [30].

The other trap-assisted transport mechanism is TAT in which electrons first tunnel from the gate-metal to a band of localized traps in the barrier, followed by tunneling to the GaN channel. According to this process, the current density can be expressed by [28]:

$$J_{TAT}(P, T, m) = \frac{q}{E_b(P, T, m)} \int_0^{\phi_{t-2}} \left( \frac{1}{R_1(P, T, m, \phi)} + \frac{1}{R_2(P, T, m, \phi)} \right)^{-1} d\phi \quad (28)$$

in which  $R_1$  and  $R_2$  represent tunneling rates from metal to the lower edge of the localized trap band and from the higher edge of the trap band ( $\phi_{t-2}$ ) to 2DEG, respectively. According to Karmalkar *et al.*,  $R_1$  and  $R_2$  are determined as functions of  $E$ ,  $N_t$ , and barrier heights for the trap states (PF and TAT) [28].

### 5. Results and Discussion

In this paper, an Analytical-Numerical model is presented for reverse gate leakage current in AlGaIn/GaN high electron mobility transistors to investigate the influence of the hydrostatic pressure. To obtain a self-consistent solution of basic equations, iteration between the Schrödinger–Poisson equation systems is conducted by a three-point finite difference method. During the self-consistent calculation, A grid spacing is as small as  $1 \times 10^{-10} m$

threshold voltage on the pressure at different temperatures, indicating that the increases in pressure cause an increase of the absolute threshold voltage. In fact, the threshold voltage depends on the density of the bound charge at the heterointerface ( $\sigma_b$ ). Increasing the hydrostatic pressure in the range of 0-5 GPa leads to the  $\sigma_b$  increase to  $1.3 C/m^2$  (Fig. 2). According to Figure 2, the reason for the increase in  $\sigma_b$  with pressure

$$|V_T|$$

$$6 \times 10^{16} m^{-2} \text{ to } 6.8 \times 10^{16} m^{-2}$$

( $E_b$ ) shown in Eqs. 25-28. As

shown in Figure 5, up to the threshold voltage ( $V_T = 3.8V$  in 0GPa, where the density is almost zero), the barrier electric field is constant and is equal to  $2.68 \times 10^8 V/m$  in 0GPa. At  $V_{GS} > V_T$ , the barrier electric field (as described in Eq. 22) decreases to  $1.2 \times 10^8 V/m$  with increasing electron density to  $6.1 \times 10^{16} m^{-2}$

( $I_{FN}$ ) in terms of gate-source voltage at different pressures. As hydrostatic pressure increases to 2 GPa, the FN tunneling current increases to  $2.4 \times 10^{-7} A$  and the horizontal region (which is FN dominant) decreases to 1.15V. In fact, the process of changes in the FN tunneling current is the same as that of changes in the barrier electric field ( $E_b$ ) and is inversely proportional to Schottky barrier-height ( $\phi_B$ ) as shown in Fig 5. These are verified by the  $I_{FN}$  relationship as described in Eq. 25. Figure 7 shows the  $I_{TAT}$  and  $I_{PF}$  currents in terms of gate-source voltage at different pressures. In this Figure, the dominant current is  $I_{PF}$  up to the turning point ( $V_G = -1.25V$ ). As the pressure increases by 2 GPa, the turning point moves to +1 volts and the range  $I_{PF}$  increases 56% relative to  $I_{TAT}$ . In general, the effect of hydrostatic pressure on the  $I_{PF}$  is greater than that on  $I_{TAT}$ . The important contribution of these changes is related to the dependence of  $I_{PF}$  on the Coulomb interaction, which in turn depends on the changes in the AlGaIn electric field. As shown in Finger 8, the larger the electric field, the stronger the interaction and the greater the  $I_{PF}$ . In general, as hydrostatic pressure increases to 2 GPa (in  $E_b = 1.8 \times 10^8 V/m$ ),  $I_{PF}$  and  $I_{TAT}$  increase to  $0.9 \times 10^{-8} A$  and  $0.1 \times 10^{-8} A$ ,

respectively, thus  $I_{PF}$  is greater than  $I_{TAT}$ . In this figure, the dependence on the electric field of  $I_{PF}$  and  $I_{FN}$  is more than  $I_{TAT}$ . A comparison of Figure 8 and its Insert reveals that all currents increase with increasing pressure, and currents that are more dependent on the AlGaIn electric field (i.e., their polarization and density in Eq. 22) are more dependent on pressure. To compare the results with experimental data, the typical gate-current is as shown in Figure 9. The inserted figure shows the variations of the total gate current relative to the voltage at different pressures. As hydrostatic pressure increases to 2 GPa, the reverse gate current increases by an average of 35%, and the threshold voltage increases to 1.15 V in absolute terms. In other words, the increase in hydrostatic pressure acts as a positive virtual gate. As explained in the last part of the introduction, thermionic field-emission plays a smaller role, which is neglected in this model at a low temperature range.

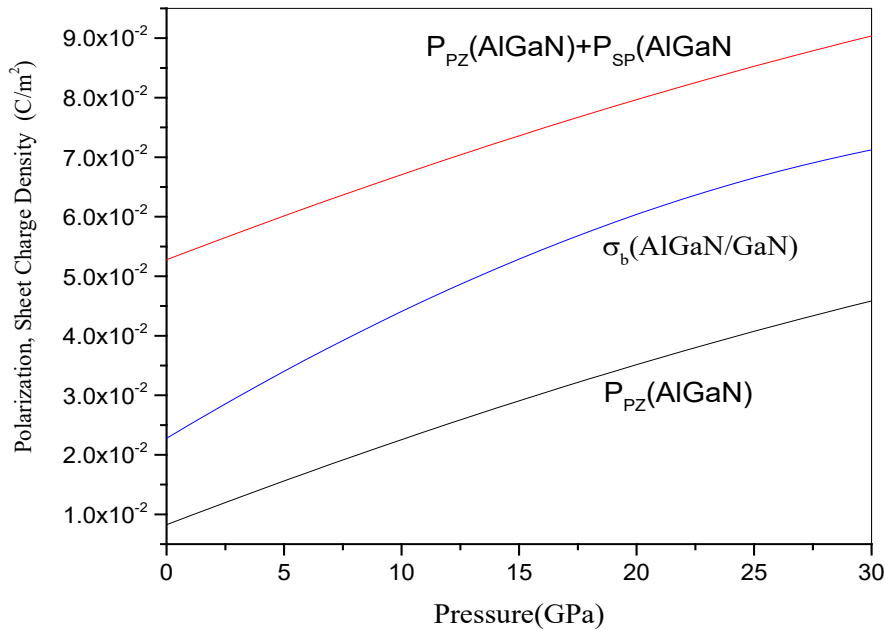


Fig. 2 - The variation of AlGaIn polarization (Piezoelectric and spontaneous) and bound charge at the hetrointerface ( $\sigma_b$ ) as a function of the hydrostatic pressure

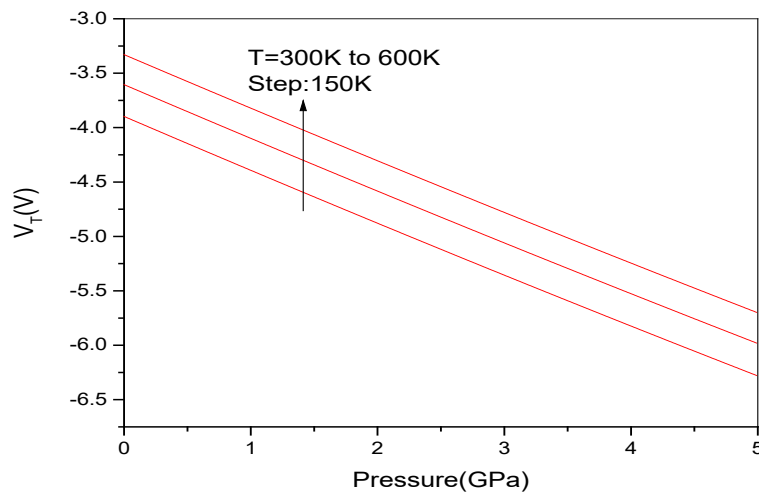
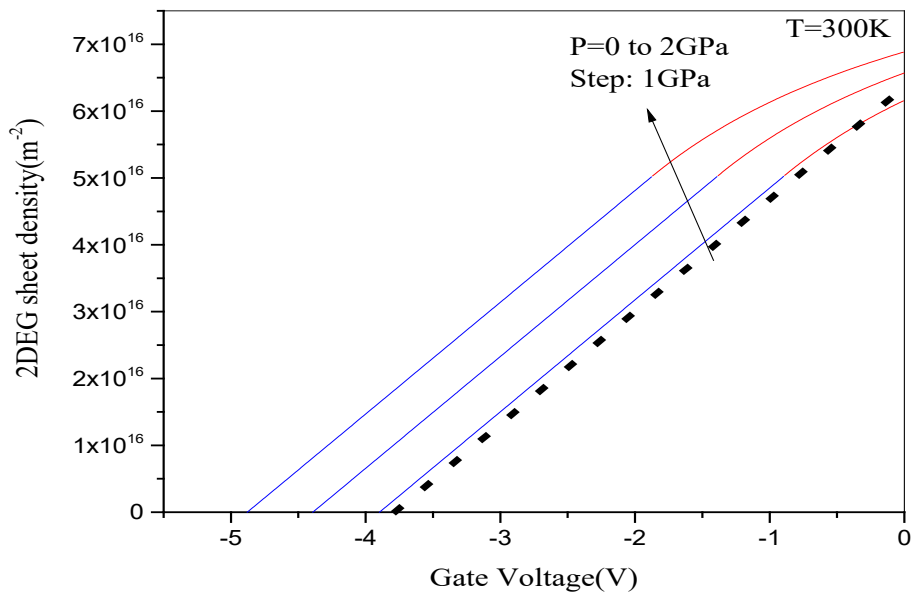
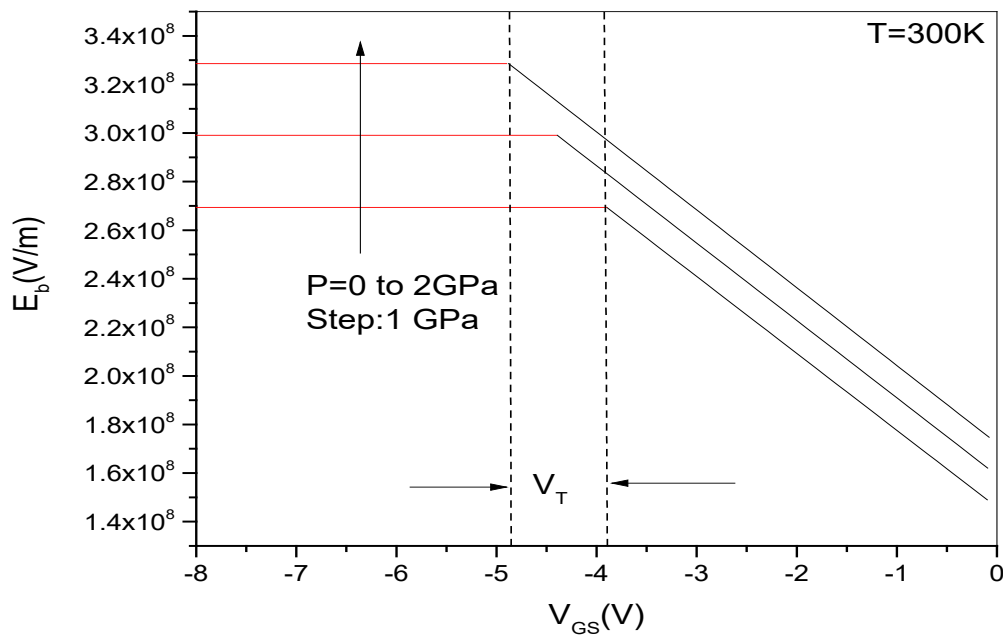


Fig. 3 - The variations of the threshold voltage as a function of the hydrostatic pressure at different temperatures



**Fig. 4 - Variations of the 2DEG sheet density as a function of Gate source voltage at different hydrostatic pressures. Insert: variations of the 2DEG sheet density as a function of Gate source voltage at different temperatures. The experimental data (symbols) and other needed parameters have been taken from Ref. [9]**



**Fig. 5 - Variations of the electric field in the AGaN layer as a function of Gate source voltage at different hydrostatic pressure**



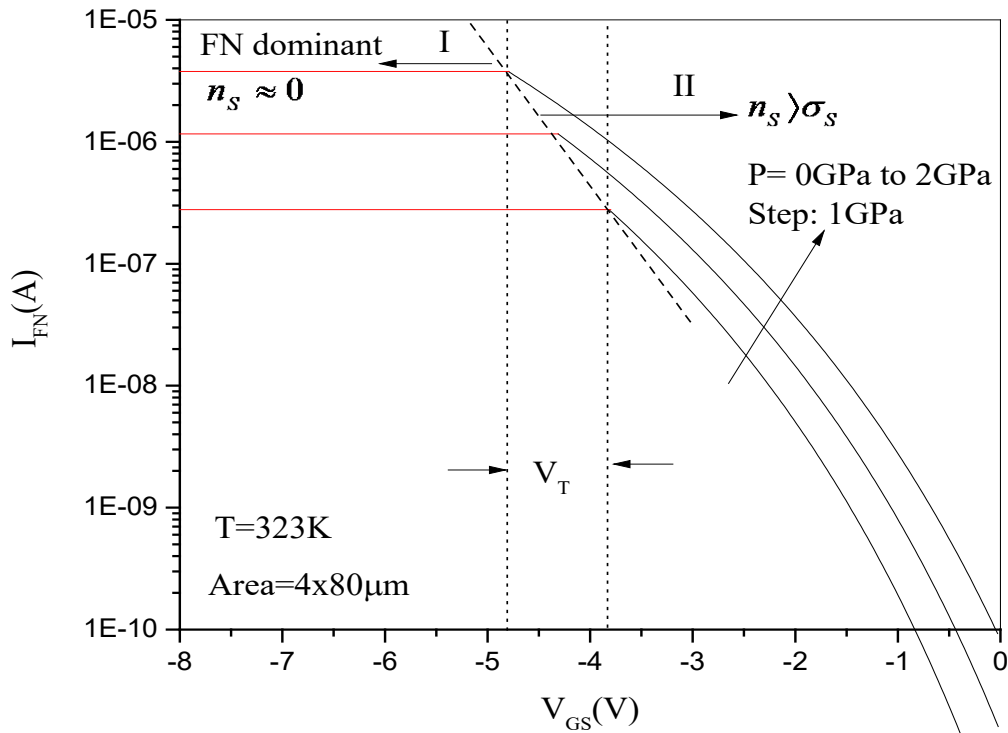


Fig. 6 - Variations of the FN tunneling current density as a function of Gate source voltage at different hydrostatic pressure

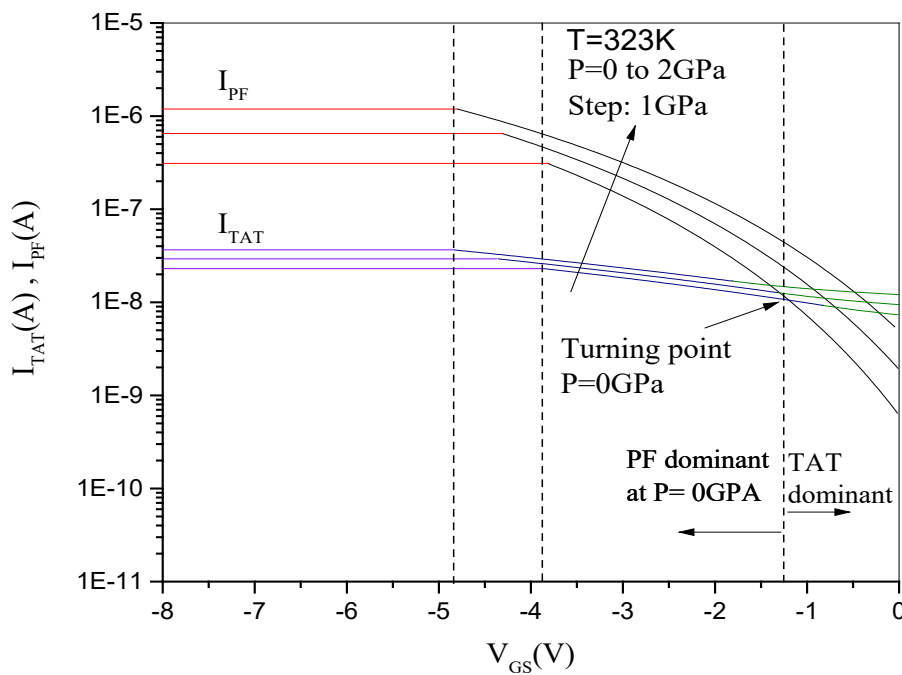


Fig. 7 - Variations of the  $I_{TAT}$  and  $I_{PF}$  currents in terms of gate-source voltage at different hydrostatic pressure

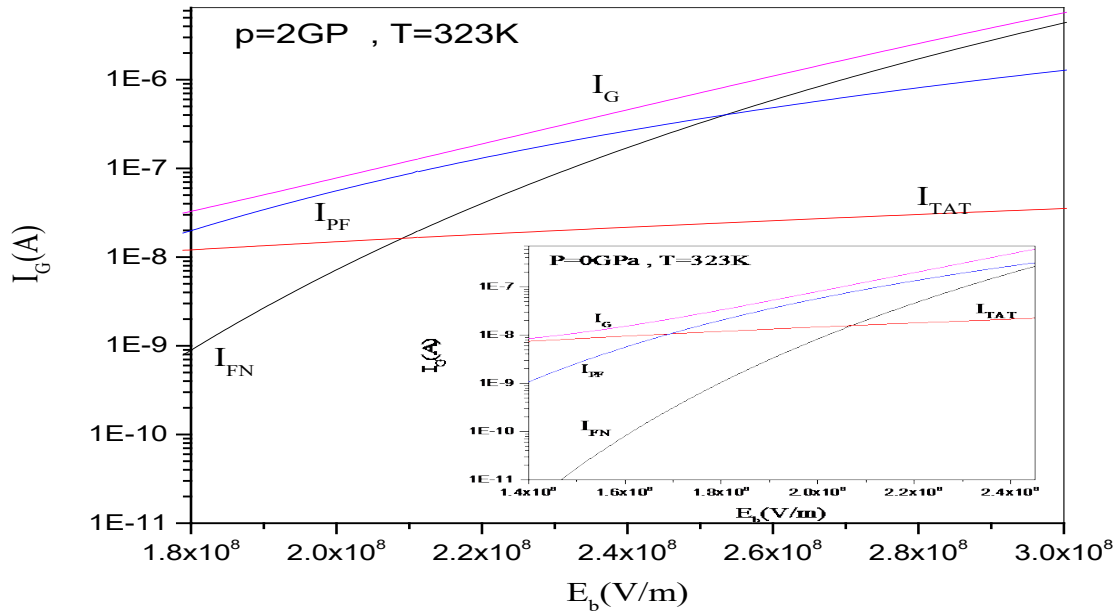


Fig. 8 - PF, FN, and TAT current components in terms of  $E_b$  at 2 GPa,  $T=323K$  and  $V_{D_s} = 0$ . The Gate-current ( $I_G$ ) curve is the sum of three components. Insert: the variations revers gate-current relative to  $E_b$  at 0GPa pressures

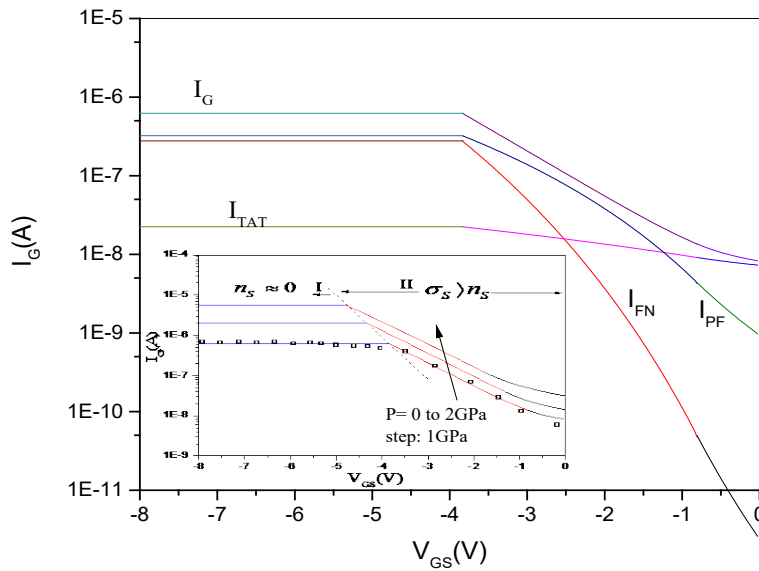


Fig. 9 - PF, FN, and TAT current components in terms of  $V_{GS}$  at 0GPa,  $T=323K$  and  $V_{D_s} = 0$ . The Gate-current ( $I_G$ ) curve is the sum of three components. Insert: the variations revers gate-current relative to  $V_{GS}$  at different pressures. The experimental data (symbols) and other needed parameters have been taken from Ref [9]

## 6. Conclusion

An analytical-numerical model for gate leakage current was investigated in AlGaIn/GaN high electron mobility transistors. An increase in pressure causes an increase of the absolute threshold voltage. With increasing pressure, the gate leakage current increases and the sub-threshold region ( $V_{GS} < V_T$  that are NF and PF dominant) decreases. Increasing the hydrostatic pressure, in the range of 0-2 GPa leads to (I)  $\sigma_b$  increases to  $0.4 \text{ C/m}^2$ , (II) the electron density increases to  $0.8 \times 10^{16} \text{ m}^{-2}$ , (III) FN tunneling current increases to  $2.4 \times 10^{-7} \text{ A}$ , (IV) in  $E_b = 1.8 \times 10^8 \text{ V/m}$ ,  $I_{PF}$  increases to  $0.9 \times 10^{-8} \text{ A}$  and  $I_{TAT}$  to  $0.1 \times 10^{-8} \text{ A}$ , and (V), the reverse gate current increases by an average of 35%. In other words, the increase in hydrostatic pressure acts as a positive virtual gate. With increasing pressure,  $I_{PF}$  is generally higher than  $I_{TAT}$  and the dependence on the electric field of  $I_{PF}$  and  $I_{FN}$  is more than  $I_{TAT}$ . By increasing the pressure of 2 GPa, the intersection point of PF and TAT currents (turning point) varies by 1 volt, and the PF range increases compared to TAT. The calculated results for electron density and gate-current are in good agreement with existing experimental data.

## Acknowledgement

The authors would like to thank Khoy Branch (Islamic Azad University) for the financial support of this research, which is based on the research project contract.

## References

- [1] K.W. Jang, I.T. Hwang, H.J. Kim, S.-H. Lee, J. Lim, H.S. Kim. (2020). Thermal Analysis and Operational Characteristics of an AlGaIn/GaN High Electron Mobility Transistor with Copper-Filled Structures: A Simulation Study. *Micromachines*, 11(1), 53-66
- [2] R. Yahyazadeh, Zahra hashempour. (2019). Numerical Optimization for AlGaIn/GaN HEMTs Including polarization coulomb Field Scattering. *Journal of Non –Oxide Glasses*, 11(2), 19-26
- [3] R. Yahyazadeh, Zahra hashempour. (2019). Effects of Hydrostatic Pressure and Temperature on the AlGaIn/GaN High Electron Mobility Transistors. *Journal of Interfaces, Thin films, and Low dimensional systems*, 2, 183-194
- [4] R Yahyazadeh, Z. Hashempour. (2019). Numerical Optimization for Source-Drain Channel Resistance of AlGaIn/GaN HEMTs. *Journal of Science and technology*, 11(1), 1-9
- [5] C Jiang et al. (2017) Piezotronic effect tuned AlGaIn/GaN high electron mobility transistor. *Nanotechnology*, 28, 455203.
- [6] O. Mitrofanov and M. Manfra. (2004). Poole-Frenkel electron emission from the traps in AlGaIn/GaN transistors. *J. Appl. Phys*, 95(11), 64149
- [7] M. Houssa, M. Tuominen, M. Naili, V. Afanas'ev, A. Stesmans, S. Haukka, and M. M. Heyns. (2000). Trap-assisted tunneling in high permittivity gate dielectric stacks," *J. Appl. Phys.*, 87(2), 861520
- [8] H. Rahbardar Mojaver and P. Valizadeh. (2016). Reverse Gate-Current of AlGaIn/GaN HFETs: Evidence of Leakage at Mesa Sidewalls. *IEEE Transactions on Electron Devices*, 63(4), 1444-1449
- [9] S. Turuvekere, N. Karumuri, A. A. Rahman, A. Bhattacharya, A. DasGupta, N. DasGupta. (2013). Gate leakage mechanisms in AlGaIn/GaN and AlInN/GaN HEMTs: Comparison and modeling. *IEEE Transactions on Electron Devices*, 60(10), 3157-3165
- [10] C. Jiang, T. Liu, C. Du, X. Huang, M. Liu, Z. Zhao, L. Li, X. Pu, J. Zhai, W. Hu, Z. L. Wang. (2017). Piezotronic effect tuned AlGaIn/GaN high electron mobility transistor. *Nanotechnology*, 28, 455203
- [11] I. Vurgaftman, J. R Meyer, L. R. R Mohan. (2001). Band parameters for III–V compound semiconductors and their alloys. *J. Appl. Phys*, 89, 5815
- [12] K.J Bala, A. J Peter, and C. W Lee. (2017). Simultaneous effects of pressure and temperature on the optical transition energies in a Ga<sub>0.7</sub>In<sub>0.3</sub>N/GaN quantum ring. *Chemical Physics*, 495, 42
- [13] R. Yahyazadeh, Zahra hashempour. (2020). Numerical Performance of AlGaIn/GaN High Electron Mobility Transistors under Hydrostatic Pressure and Temperature. *Journal of Science and technology*, 12(1), 15-28
- [14] Z. Dridi, B. Bouhafs, Ruterana. (2002). Pressure dependence of energy band gaps for Al<sub>x</sub>Ga<sub>1-x</sub>N, In<sub>x</sub>Ga<sub>1-x</sub>N and In<sub>x</sub>Al<sub>1-x</sub>N. *New Journal of Physics*, 4, 1.1–1.15
- [15] O. Ambacher, B. Foutz, J. Smart, J. R. Shealy, N. G. Weimann, K. Chu, M. Murphy, A. J. Sierakowski, W. J. Schaff, L. F. Eastman. (2000). Two dimensional electron gases induced by spontaneous and piezoelectric polarization in undoped and doped AlGaIn/GaN heterostructures. *Journal of Applied Physics*, 87, 334
- [16] O Ambacher, J Majewski, C Miskys, A Link, M Hermann, M Eickhoff, M Stutzmann, F Bernardini, V Fiorentini, V Tilak, B Schaff and L F Eastman. (2002). Pyroelectric properties of Al (In) GaN/GaN hetero- and quantum well structures. *J. Phys. Condens. Matter*, 14, 3399

- [17] Z. J. Feng, Z. J. Cheng, and H. Yue. (2004). Temperature dependence of Hall electron density of GaN-based heterostructures. *Chinese Physics*, 13, 1334
- [18] V. Fiorentini, F. Bernardini, and O. Ambacher. (2002). Evidence for nonlinear macroscopic polarization in III-V nitride alloy Heterostructures. *Appl. Phys. Lett.*, 80, 1204
- [19] P. Perlin, L. Mattos, N. A. Shapiro, J. Kruger, W. S. Wong, T. Sands, N. W. Cheung, and E. R. Weber. (1995). Reduction of the energy gap pressure coefficient of GaN due to the constraining presence of the sapphire substrate. *Journal of Applied Physics*. 85, 2385
- [20] K. elibol, G. Atmaca, P. Tasli, S.B.Lisesivdin. (2013). A numerical study on subband of InxAl1-xN/InN-based HEMT structure with low-indium ( $x < 0.01$ ) barrier layer.” *Solid state communication*, 162, 8-12
- [21] R. Yahyazadeh. (2018). Analytical-numerical model for sheet resistance of AlGaIn/GaN high electron mobility transistors, *Journal of Non - Oxide Glasses*.10, 57 – 63
- [22] P. Roblin, H. Rahdin. (2002) “High-speed Heterostructure Devices from Device Concepts to Circuit Modeling.” Cambridge University Press, Cambridge.277
- [23] A .Agrawal, M .Gupta, R. S. Gupta. (2009). RF performance assessment of AlGaIn/GaN MISHFET at high temperatures for improved power and pinch-off characteristics. *Micro. Opt. Techn. Letter*, 51, 1942
- [24] C. M. Duque, A. L. Morales, M. E. Mora-Ramos, and C. A. Duque. (2015). Exciton-related optical properties in zinc-blende GaN/InGaIn quantum wells under hydrostatic pressure. *Physica Status Solidi (b)*, 252, 670
- [25] M. Yang et al. (2016). Effect of polarization coulomb field scattering on parasitic source access resistance and extrinsic transconductance in AlGaIn/GaN heterostructure FETs. *IEEE Trans. Electron Devices*, 63, 1471–1477
- [26] A. F. M. Anwar, R. T. Webster, and K. V. Smith. (2006). Bias induced strain in AlGaIn/GaN heterojunction field effect transistors and its implications *Appl. Phys. Lett*, 88, 203510
- [27] Karumuri et al. (2014). A continuous analytical Model for 2-DEG Charge Density in AlGaIn/GaN HEMTs Valid for All Bias Voltage. *IEEE Transactions on Electron Devices*, 61(7), 2343-2349
- [28] S. Karmalkar, D. M. Sathaiya, and M. S. Shur, (2003). Mechanism of the reverse gate leakage in AlGaIn/GaN high electron mobility transistors. *Appl. Phys. Lett.*, 82(22), 3976-3978
- [29] H. Zhang, E. J. Miller, and E. T. Yu. (2006). Analysis of leakage current mechanisms in Schottky contacts to GaN and Al<sub>0.25</sub>Ga<sub>0.75</sub>N/GaN grown by molecular-beam epitaxy. *J. Appl. Phys.*, 99(2), 023703-1–023703-6
- [30] A. Wang, L. Zeng, W. Wang. (2017). Simulation of gate leakage current of AlGaIn/GaN HEMTs: Effects of the gate edges and self-Heating” *ECS Journal of solid state science and Technology*, 6(11), 3025-3029